Electronic Supplementary Material (ESI) for Energy & Environmental Science.

Supporting Information

Balancing Electron Transfer Rate and Driving Force for Efficient Photocatalytic Hydrogen Production in CdSe/CdS Nanorod-[NiFe] Hydrogenase Assemblies

Bryant Chica,[†] Chang-Hao Wu,[‡] Yuhgene Liu,[†] Michael W.W. Adams,[¶] Tianquan Lian,[†] and R. Brian Dyer*[,†]

[†]Department of Chemistry, Emory University, Atlanta GA, USA
[‡]Department of Chemistry and Biochemistry, University of Georgia, Athens GA, USA
[¶]Department of Biochemistry and Molecular Biology, University of Georgia, Athens GA, USA
*Corresponding Author: briandyer@emory.edu

SI.0 Ordering of energy levels in Scheme 1 Diagram

The relevant energy levels for catalysis and electron transfer in scheme 1. The energy of the CdSe valence band was taken as the lowest energy electronic state measured in a previous study[1] of hole transfer using CdSe/CdS core-shell quantum dots referenced to ferrocene/ferrocenium redox couple and converted to the NHE[2] scale. The CdS and CdSe conduction bands were offset by 300 meV which is the generally agreed upon value in these nano-heterostructures with quasi-type II band alignment.[3-5] The valence bands were located by measuring the energies of the onset of absorption by the CdSe seed and CdS rod from the optical spectra (Figure SI.0). The reduction potential of the cysteine sacrificial electron donor is taken from a recent work characterizing the reduction potential of biological thiols.[6]

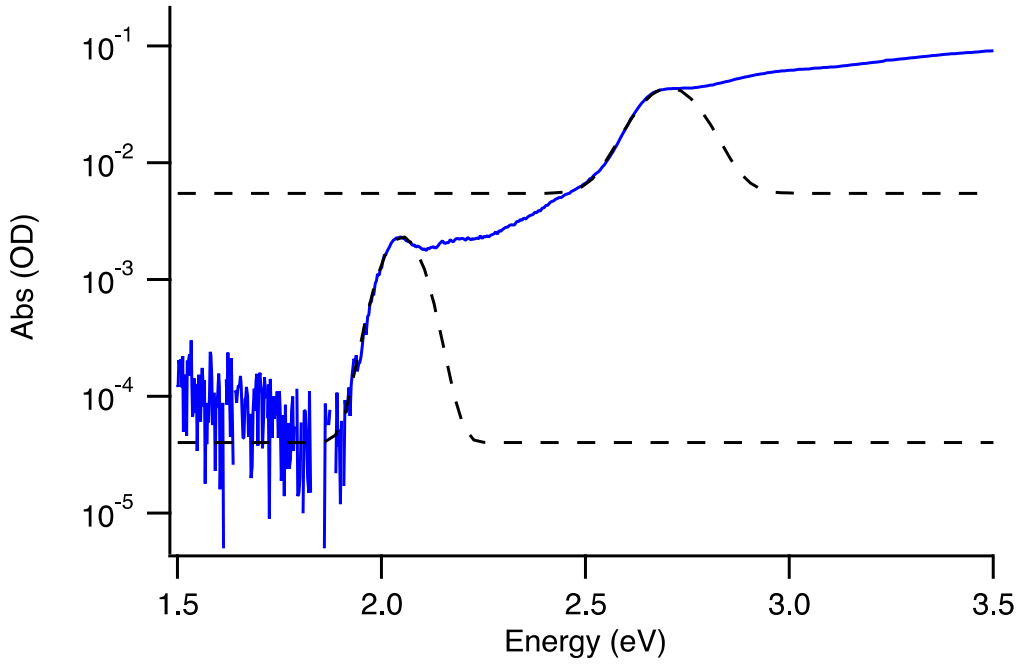

Figure SI.0 Band edges of CdSe/CdS DIR. Ground state optical absorption spectrum of CdSe/CdS DIRs with Gaussian fits to the CdSe absorption onset (2.0496 $\pm$ 0.0005 eV) and the CdS absorption onset (2.705 $\pm$ 0.001 eV)

SI.1 *Pf* SHI Structure and Interaction with CdSe/CdS DIR

Pf SHI-DIR complexes were not photocatalytically active for hydrogen generation at room temperature when assembled as detailed in the experimental section with the exception of the absence of a redox mediator.
We suspect, that the poly-histidine tag, included for purification purposes, enforces a nanoparticle-protein interaction geometry that is unproductive for excited state electron transfer. Interaction of poly-histidine motifs with metal and semiconductor surface has been explored in detail by other groups[7, 8] who have shown that histidine tagged proteins bind very strongly to quantum dot surfaces with binding constants on the order of ~1- 5 nM^{-1}. Figure SI1 shows a schematic of the proposed interaction of hetero-tetrameric *Pf* SHI with the surface of the CdSe/CdS DIR. The 9x-histidine tag is appended to the β-subunit as depicted in figure SI2.1. The location of the his-tag on the β-subunit of the hetero-tetrameric SHI[9] will cause the interaction with the DIR surface to be localized at that subunit. The β-subunit is not thought to be functional for ET to exogenous redox partners, but rather for transporting electrons within the tetramer between the diaphorase γ-subunit and the FeS clusters of the δ-subunit and ultimately to the α-subunit that houses the [NiFe] active site. Excited state ET from DIR to SHI would require that one of the FeS clusters of the γ, β or δ subunits must be relatively solvent exposed and have nearby basic residues to promote strong electrostatic interaction with the CdS surface. Unfortunately, the lack of a crystal structure for this enzyme means the detailed location and environment of the FeS clusters is not known and the rational design of a direct pathway for interfacial electron transfer is difficult.

In any case, the lack of more specific knowledge about the SHI-DIR interaction is not crucial to understanding the other results presented in this paper. The primary pathway of electron transfer between the DIR and the SHI is through a soluble redox mediator, which should not depend strongly on the properties of the SHI-DIR interface

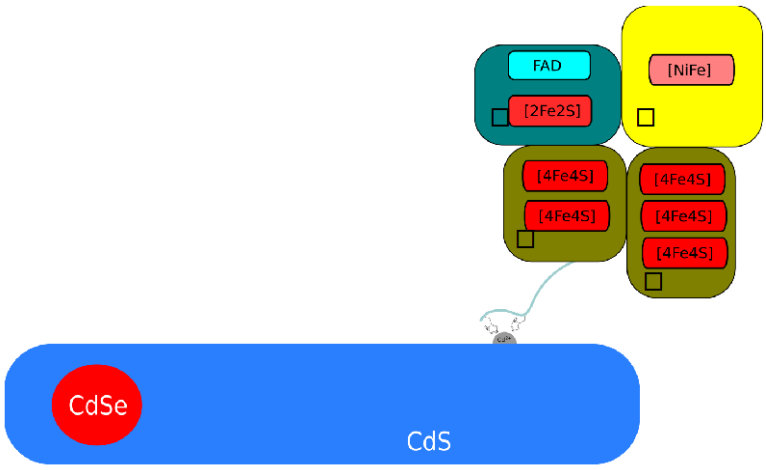

Figure SI.1 – **Depiction of the *Pf* SHI – DIR interaction** mediated by the 9x histidine tag on the β-subunit of the enzyme.

SI.2 Langmuir Isotherm Fitting

Fluorescence measurements were taken on a Flouromax spectrophotometer (Horiba Scientific, Edison, New Jersey). Optical densities of the CdSe/CdS DIR at the excitation wavelengths were kept below 0.1 to minimize inner filter effects. Samples of the DIR were prepared in 50mM phosphate buffer in an anaerobic chamber and loaded into a quartz fluorescence cuvette (Starna Cells) sealed with a septum. Concentrated solutions of the redox mediators were titrated in via gas tight syringe (Hamilton) to generate the appropriate mediator concentrations with minimal dilution (>1% throughout). The excitation monochromator was set to 450 nm. The CCD detector was set to low gain with 10 milliseconds integration time to avoid saturation of the detector and each spectrum was the result of 3 averages.

The PL titrations in Figure 1B were fit to the following modified Langmuir isotherm:

$$\frac{PL}{PL_0} = Q_{pre} + Q_{max}\left(1 - \frac{k_{lang}c_{mediator}}{1 + k_{lang}c_{mediator}}\right)$$

Here PL is the integrated PL intensity at a particular redox mediator concentration, $c_{mediator}$. PL_0 is the integrated PL intensity in the absence of redox mediator. K_{lang} is the Langmuir binding constant and Q_{max} is a parameter that dictates the maximum level of PL quenching observed. Q_{pre} accounts for any offset occurring at the initial high dilution points.

Table S1: Parameters for Langmuir isotherms in Figure 1B

Condition	K_{lang} M^{-1}	$1/K_{Lang}$ (μM)
MV titration	28661	34.9uM
PDQ titration	13044	76.7uM
MV titration, 16 mM Cys	5593	179uM
PDQ titration, 16 mM Cys	2941	340uM

SI.3 Quantum yield of Mediator Reduction

Quantum yield of mediator photoreduction was determined by controlled photoexcitation of samples containing CdSe/CdS DIR, redox mediator and sacrificial electron donor (100mM Cysteine) in 50mM phosphate buffer pH = 7 in a septum sealed fluorescence cuvette (Firefly Scientific). Sample volume was 3.5 mL and PDQ^{2+} or MV^{2+} concentrations were 8 mM. Prior to the experiment the cuvette headspace was purged with N_2 gas for 20 minutes. Samples were exposed to 4.04 mW 405 nm light from a diode laser gated by a mechanical shutter in cycles of 10 s open 10 s closed under vigorous magnetic stirring. Real time in-situ monitoring of the radical concentration was performed with a fiber coupled UV-Vis spectrometer (QE 6500, Ocean Optics). Typical absorbance versus time data are presented in Figure SI.3.

The photoreduction quantum yield (QY) is calculated as:

$$QY = \frac{(moles\ mediator\ reduced\ in\ 10\ s\ illumination)}{(0.00404\ W)\left(\frac{1\ eV}{1.60218 * 10^{-19}\ W}\right)\left(\frac{405nm\ photon}{3.06\ eV}\right)(1 - 10^{-Abs_{DIR}})(100\% - 8.5\%)(10\ s)}$$

where 8.5% accounts for reflection loss of the excitation beam from front face of the cuvette. This gives initial quantum yeilds of 78% for MV^{2+} photoreduction and 89% for PDQ^{2+} photoreduction.

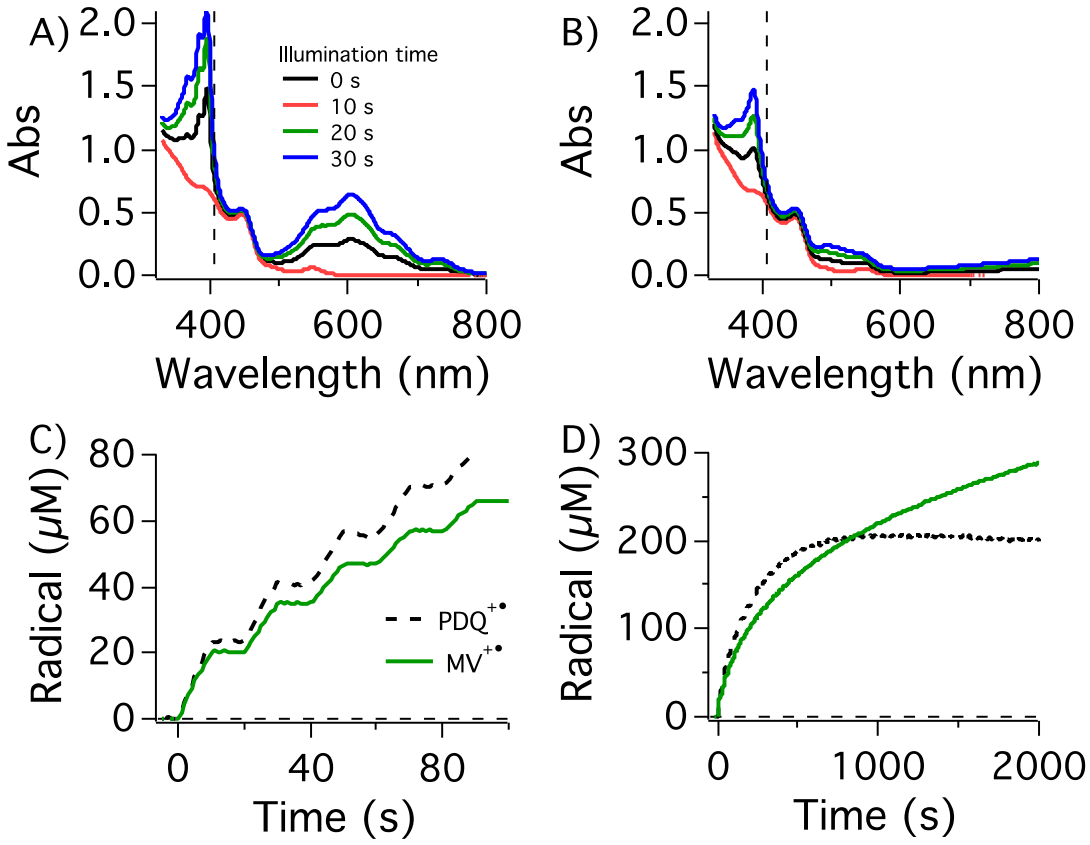

Figure SI.3 Mediator Photoreduction. Absorbance spectra as a function of time for DIR photoreduction samples with 8 mM MV^{2+} A) and 8 mM PDQ^{2+} B). Vertical dashed lines denote the energy of the excitation light. Changes in the mediator radical concentration as a function of time in the photoreduction experiment at early C) and later D) time.

SI.4 H_2 Production with MV^{2+} and PDQ^{2+} monitored by GC

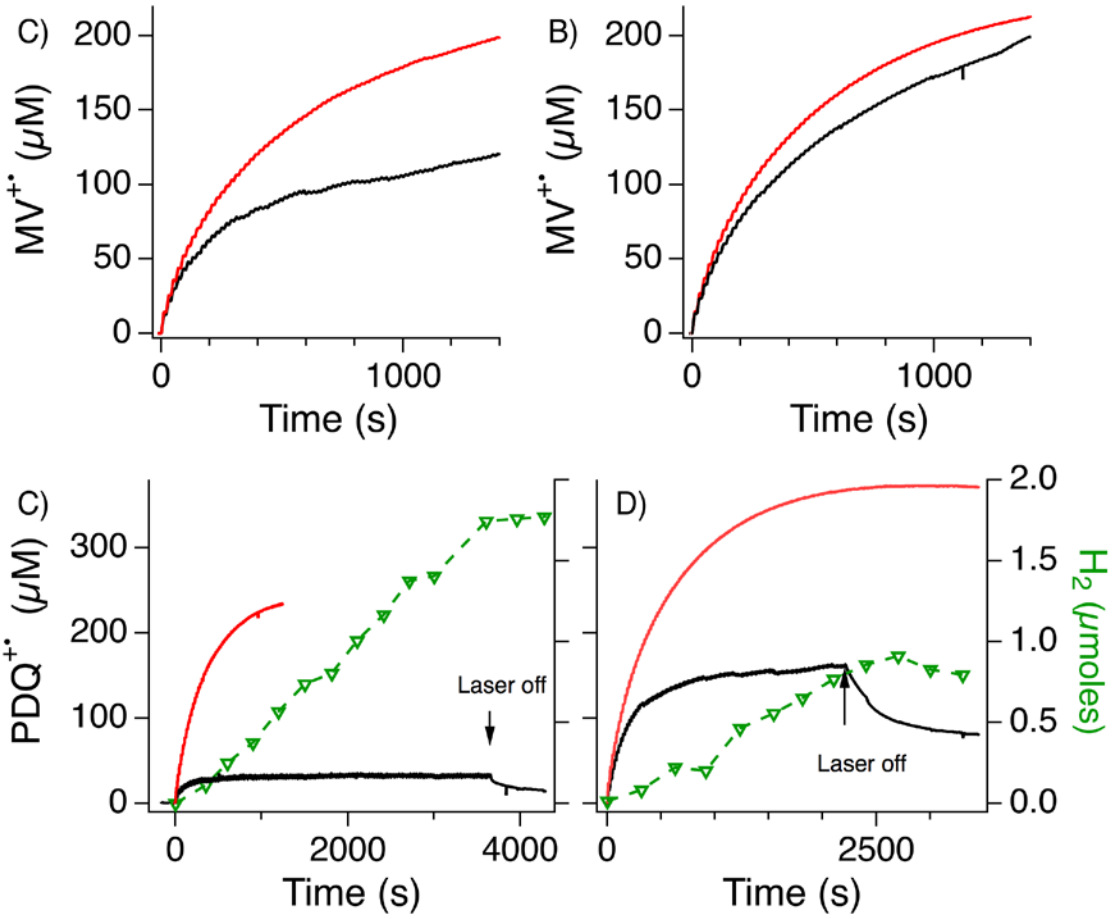

Figure SI.4. Concentration of photo-generated $MV^{+\bullet}$ (A,B) and $PDQ^{+\bullet}$ (C,D) radical in solution as a function of irradiation time at pH = 7.35 (A,C) and pH = 8.39 (B,D) with (black traces) and without (red traces) 72 nM SHI. Conditions: 5.7 mM MV^{2+} (A,B) PDQ^{2+} (C,D), 100 mM Cysteine, 12 nM MPA-DIR, 50 mM phosphate buffer, excitation source chopped 10 s on / 10 s off with a shutter. Axes on the left correspond to photogenerated radical concentration. Those on the right of the bottom panel correspond to hydrogen produced.

Calculation of H_2 production quantum yield:

The quantum efficiency of H_2 production was calculated as follows:

$$QY = \frac{2\Delta H_2}{\Delta h\nu} \quad (1)$$

Where $\Delta(H_2)$ is the initial rate of hydrogen production and $\Delta(h\nu)$ is the photon absorption rate. $\Delta(h\nu)$ is calculated from the incident power (4.04 mW) by correcting for reflection loss from the cuvette front face (8.5%). Calculating an accurate IQE requires correction for unproductive photon absorption from other species in the solution such as the catalyst or redox mediator since only photon absorption by the photosensitizer contributes to hydrogen production. In particular, PDQ radical has a non-negligible absorbance at 405 nm (ε_{405nm} = 3533 $cm^{-1}M^{-1}$) due to a steady state concentration of radical that builds up during hydrogen evolution experiments as determined by tandem UV-Vis spectroscopy (Figure 2). This can be accounted for in (1) by considering the total absorbance at 405 nm and scaling $\Delta(h\nu)$ to correct for parasitic light absorption by the PDQ radical. This changes the corrected $\Delta(h\nu)$ from (3) to (4) where P(A) is the probability of photon absorption for a measured optical absorbance (2). The value calculated using (3) is referred to as the QY in the text and the value calculated using (4) is referred to as the IQE.

$$P(A) = 1 - 10^{-A} \quad (2)$$

QY: $$\varphi = (0.00404\,W)\left(\frac{1\,eV}{1.60218 \bullet 10^{-19} W}\right)\left(\frac{405\,nm}{3.06\,eV}\right)P(A_{DIR})(100-8.5)\% \quad (3)$$

IQE: $$\varphi = (0.00404\,W)\left(\frac{1\,eV}{1.60218 \bullet 10^{-19} W}\right)\left(\frac{405\,nm}{3.06\,eV}\right)P(A_{DIR})(1-P(A_{PDQ^{\bullet}})(100-8.5)\% \quad (4)$$

This treatment gives the following efficiencies for the data in Figure SI.3:

pH = 7.35

QY: $\varphi = 41 \pm 1.5\%$

IQE: $\varphi = 52 \pm 2\%$

1.28 x 10^5 μmol H_2 (mg SHI)$^{-1}$ (hr)$^{-1}$

pH = 8.39

QY: $\varphi = 29 \pm 2\%$

IQE: $\varphi = 77 \pm 5\%$

8.97 x 10^4 μmol H_2 (mg SHI)$^{-1}$ (hr)$^{-1}$

SI.5 Quantum yield of H_2 generation from Figure 3 data

In Addition to Gas Chromatography, Hydrogen production was monitored using pressure transducers in a method inspired by the work[10] of Krauss and coworkers. Pressure transducers from Phidgets (1137_0 and 1140_0) and I/O board (1018_2) were used to monitor pressure. The sensors were cemented into cuvette caps which were sealed with o-rings. Inlets and outlets to the cells were provided by IDEX microfluidic valves to purge the cuvette headspace. Headspace volume was determined by measuring the mass of the water required to completely occupy the cuvette volume when the sample volume was present using the density of water. The ideal gas law was then used to determine the gas evolved with a correction for Henry's law that assumes equilibrium is maintained. We ensure this with vigorous stirring near the surface of the cuvette volume which we found to be necessary for lag free response of the pressure trace. ***The error in the pressure values are reported as $\pm$5% in the pressure by the manufacturer, which is directly proportional to the error in the moles of hydrogen produced.***

Table S2 – Hydrogen Production Parameters: Quantum yields, internal quantum yields and number of moles of hydrogen produced during the concentration dependent experiments reported in Figure 3.4. Values are reported measuring from the start of illumination to 1000 seconds and 2000 seconds and for the period between 1000-2000 seconds.

		Hydrogen (nanomoles)	Hydrogen (nanomoles)	PDQ radical (μM)	PDQ radical (μM)	1000s		2000s		Hydrogen nanomoles	2000s - 1000s	
[SHI] (nM)	pH	1000 s	2000 s	1000 s	2000 s	QY	IQE	QY	IQE	1000s - 2000s	QY	IQE
74	7	666	1310	37	44	0.367	0.496	0.36	0.52	644	0.36	0.51
148	7	710	1523.5	26	26	0.391	0.483	0.42	0.52	813.5	0.45	0.55
222	7	783	1626.7	23	26	0.431	0.520	0.45	0.55	843.7	0.47	0.57
74	8.2	242.8	537	105	113	0.134	0.314	0.15	0.37	294.2	0.16	0.41
148	8.2	324.2	700.8	120	129	0.179	0.474	0.19	0.55	376.6	0.21	0.59
222	8.2	343	705.5	129	142	0.189	0.539	0.19	0.62	362.5	0.20	0.63

SI.6 fs TA Spectral Evolution

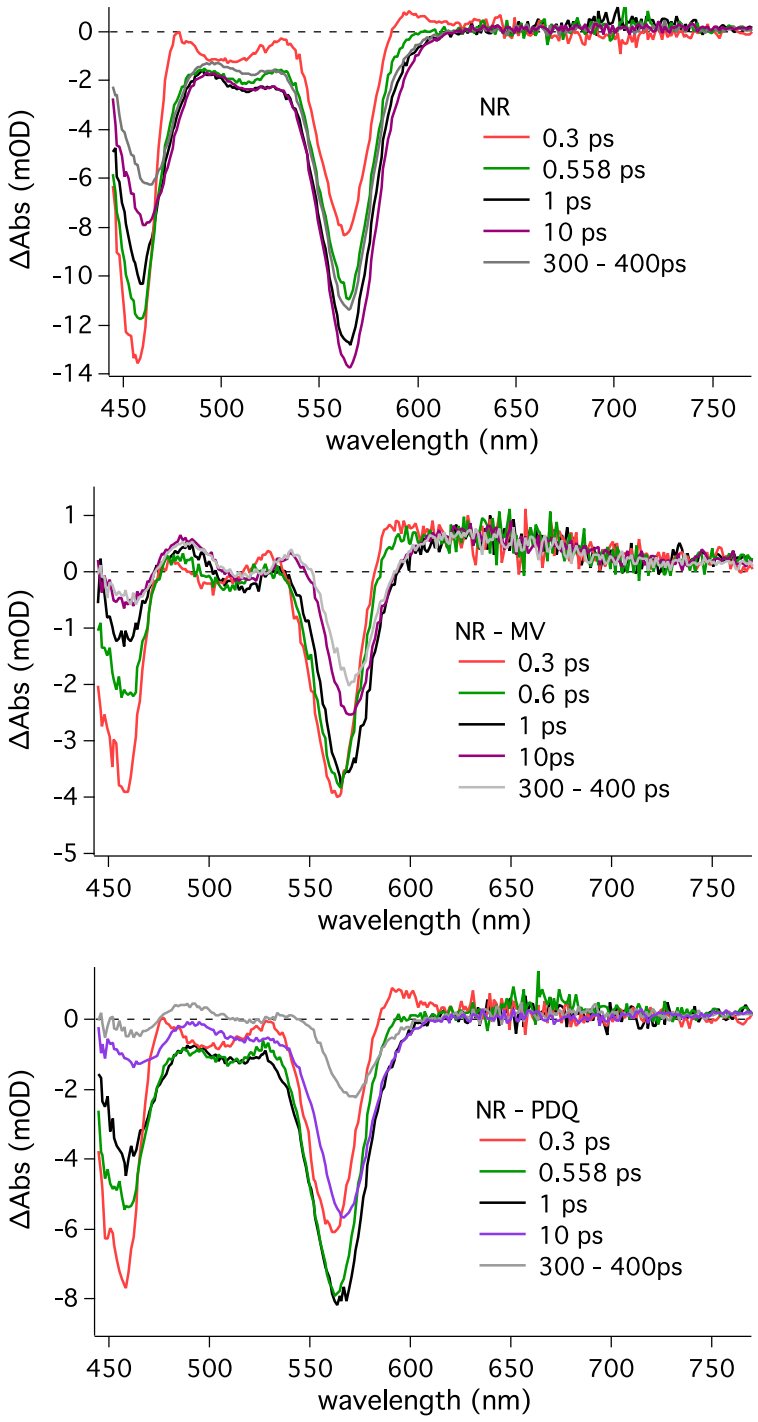

Figure SI.6. Ultrafast transient absorption spectra for DIR nanostructures (top panel) and their complexes with MV^{2+} (middle panel) and PDQ^{2+} (bottom panel). The pump-probe time delay for each spectrum is indicated in the figure legends.

SI.7 SVD Analysis of Transient Absorption data

Analysis of the transient absorption spectra were carried out in Igor Pro 6.37 using the TADataAnalysis_v4.2 code.

Errors are reported as +/- 1 standard deviation of the time constants in the multi exponential fits as output in the fitting procedure after fixing the fitted time zero, instrument response time constant and pre-excitation baseline to their fitted values.

Singular value decomposition (SVD) analysis:

Spectral regions of the nanosecond data known to contain spectral signatures of the charge separated state and excitons were selected from the nanosecond transient absorption data sets as regions of interest (ROI). SVD was performed on these ROIs and the kinetics of the singular vectors corresponding to the state of interest were extracted. The extracted singular vectors are shown in figure SI.6

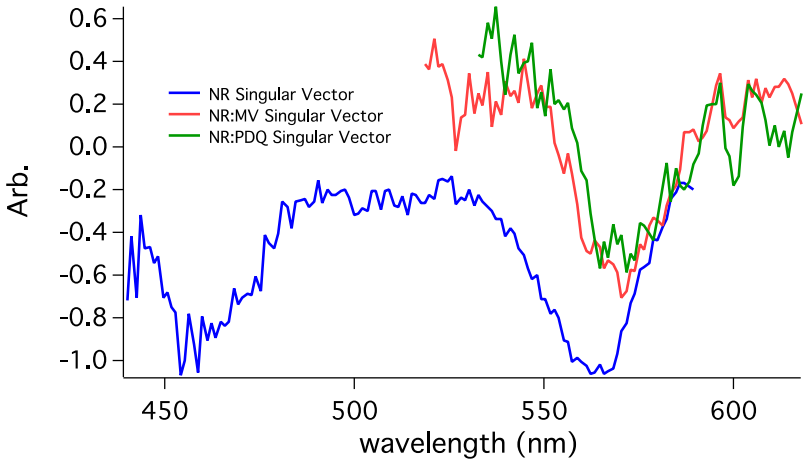

Figure SI.7. Singular vectors extracted from SVD analysis of ultrafast TA spectra. These signals reproduce the important spectral features of the exciton and charge separated states present at the end of the fs-TA experiment (Figure 3A) including the redshift of the bleaches of the charge-separated states supporting the assignment.

SI.8 Hole Transfer Dynamics

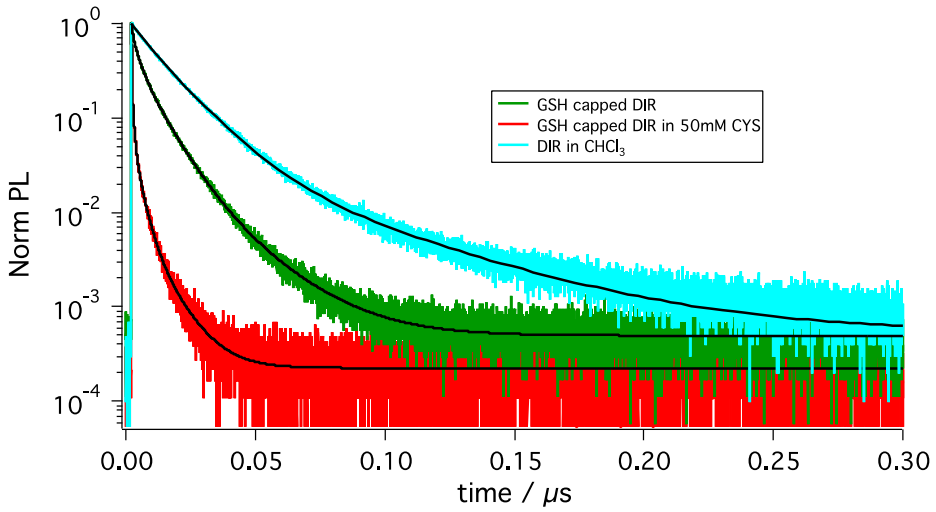

Figure SI.8. Normalized fluorescence decays of DIR fluorescence excited at 405 nm monitored by TCSPC.

The fluorescence decays in figure S4 were fit to function of the form (1) to obtain randomly distributed residuals over the whole decay trace.

$$f(t) = y_0 + \sum_{n=4} a_n \exp\left(\frac{(t-t_0)}{\tau_n}\right) \qquad (1)$$

Amplitude weighted lifetimes were the calculated for each trace by equation (2) where a_n is the amplitude of the exponential component and τ_n is the lifetime of the exponential component.

$$\tau_{awl} = \frac{\sum_n a_n \tau_n}{\sum_n a_n} \qquad (2)$$

The different surface chemistry conditions of the DIR structures are assumed to modify pathways for hole transfer from the nanostructure. Exchange of native hydrophobic ligands with the hydrophilic thiol glutathione is observed to shorten the PL decay, presumably due to transfer of holes that would normally radiatively recombine with the excited electron. Addition of 50mM cysteine to the solution shortens the lifetime consistent with its performance as a more effective sacrificial electron donor. The mechanism responsible for this dramatic difference in hole transfer between glutathione and cysteine is beyond the scope of this study but may be due to the smaller size of cysteine allowing for greater surface density of ligands to be achieved or differences in electronic structure between the two thiol ligands.

Hole transfer time can be approximated by assuming that thiol binding creates an additional channel for non-radiative decay of the fluorescence by hole transfer using the equation.

$$\tau_{HT} = \left(\frac{1}{\tau_{DIR+thiol}} - \frac{1}{\tau_{DIR}} \right)^{-1} \qquad (3)$$

Table S3. DIR hole transfer lifetimes

Sample	τ_{ht}
GSH capped DIR	7.79 ns
GSH capped DIR in 50mM Cys	0.383 ns

SI.9 pH Dependence of H_2 production rate

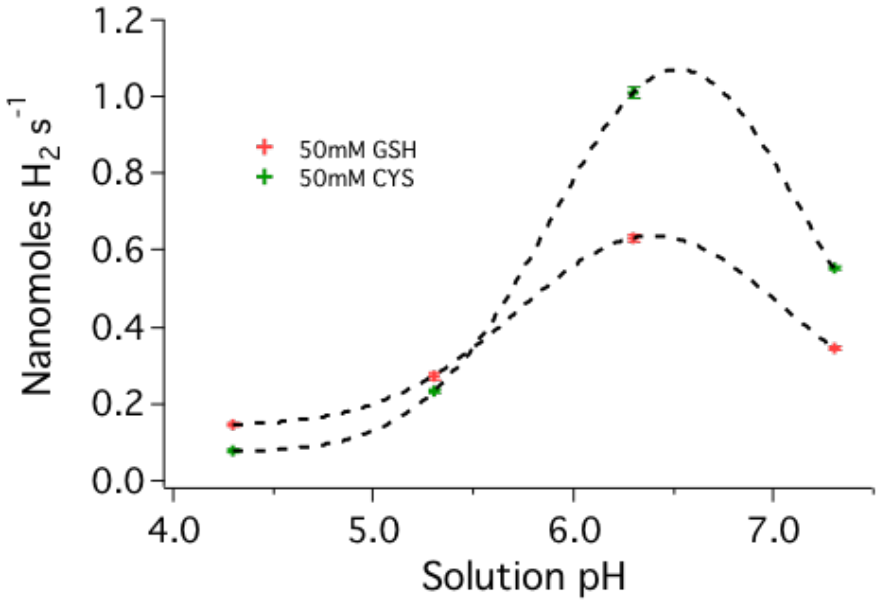

Figure SI.9. pH dependence of the H_2 production rate as a function of pH of the sacrificial donor solution. Conditions SHI = 230 nM, DIR = 12 nM, PDQ^{2+} = 50 mM, Donor = 50mM, Buffer = 50 mM Phosphate/Citrate, 4.04 mW 405 nm excitation. Fits to Gaussian functions are meant to guide the eye and do not have physical significance.

SI.10 Long term H_2 Production
(GSH CdSe/CdS DIRs)

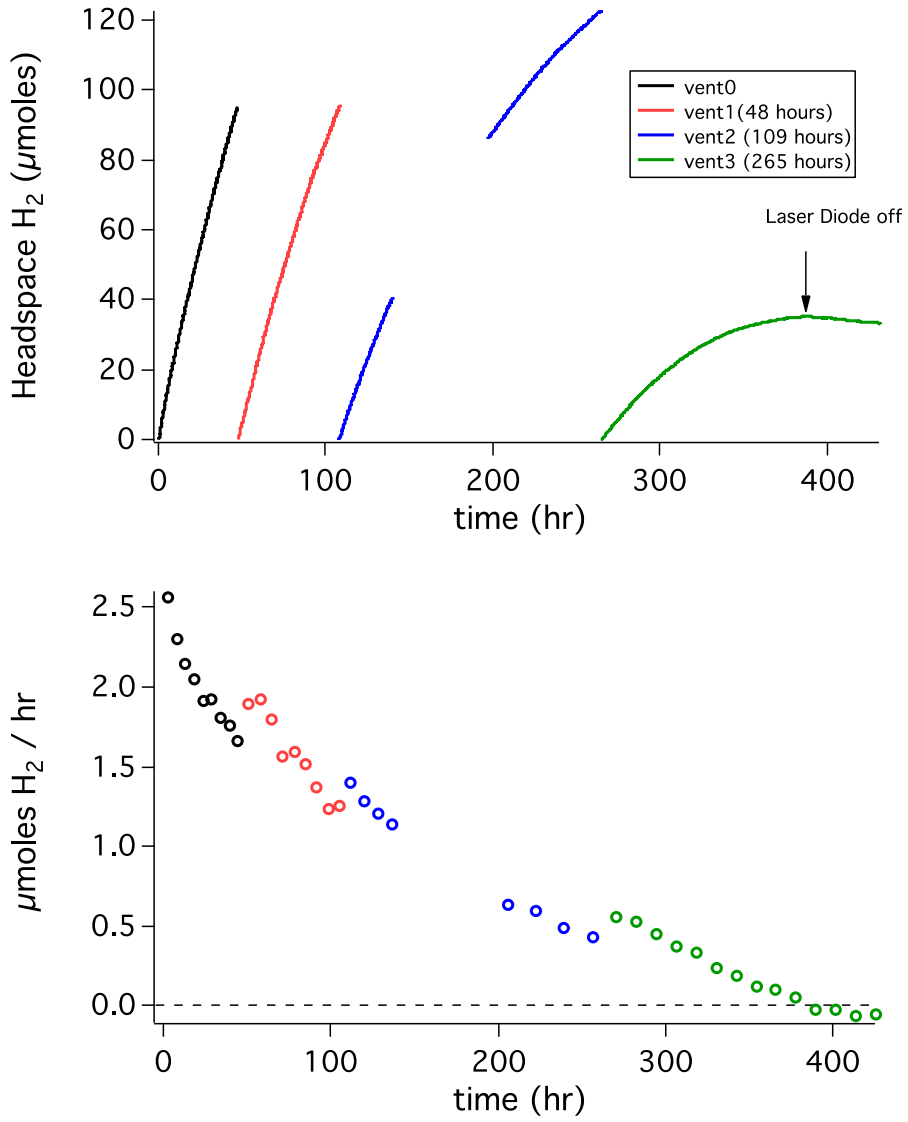

Figure SI.10. Time dependent photo-production of hydrogen from hybrid assemblies. (A) Moles of hydrogen produced, measured by headspace pressure. (B) Rate of hydrogen production as a function of illumination time. The data trace from 141-197 hours was lost due to crashing of the data collection programs, however this does not affect the measurement for hydrogen produced at other times or the yield calculated. 4.04 mW 405 nm laser diode illumination was used for these experiments. Samples prepared identically as previous photocatalysis experiments except with glutathione capped DIR and 0.5 M reduced glutathione as sacrificial electron donor.

SI.11 PDQ^{2+} Degradation Product

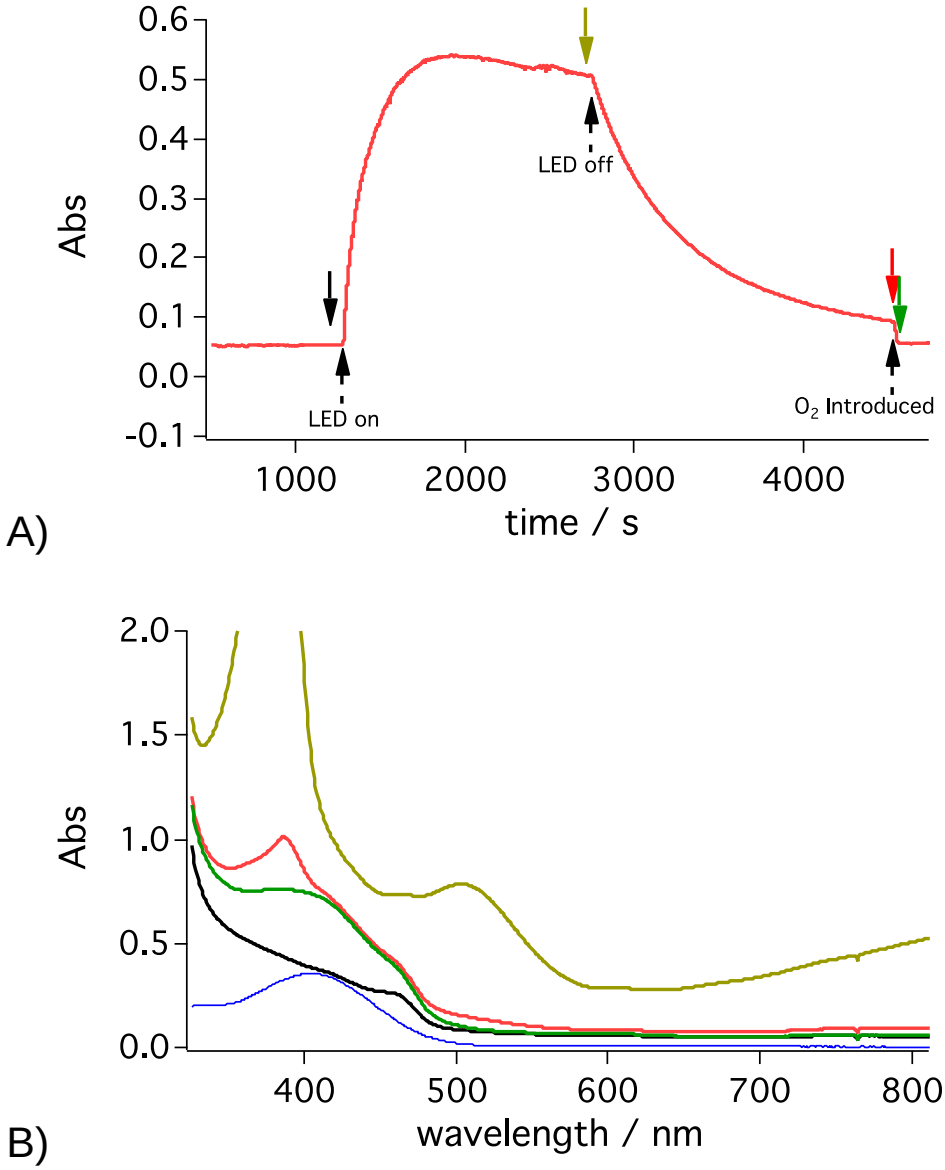

Figure SI.11. (A) Absorbance at 800 nm of glutathione capped CdS in 0.5M Glutathione pH = 6.8 with 7.14mM PDQ^{2+} under 4.04 mW 405 nm laser diode illumination. (B) Absorbance spectra at selected points from trace in panel (A) designated by downward pointing color coded arrows. The blue trace represents the difference spectrum between the sample before illumination and after quenching with oxygen, showing the buildup of the PDQ^{2+} degradation product.

SI.12 PDQ^{2+} degradation product excitation screening

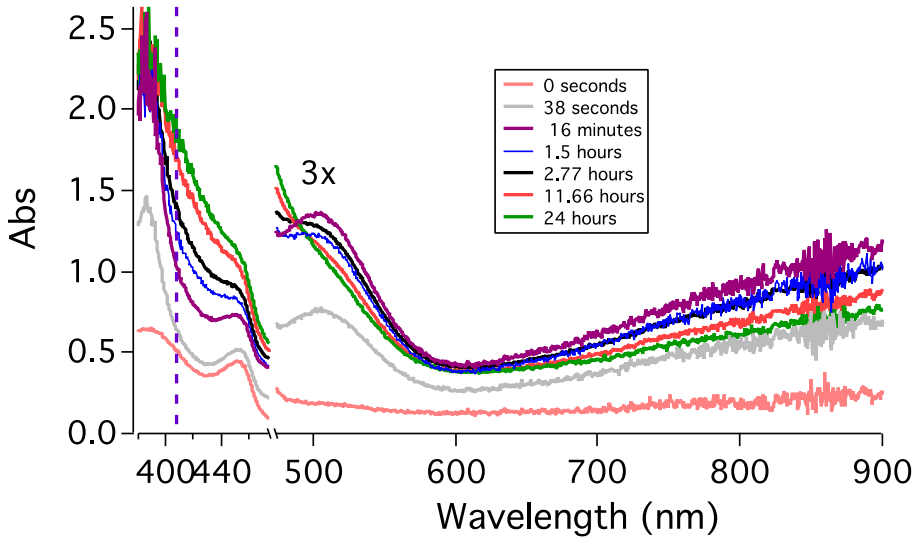

Figure SI.12A Optical spectra during a long-term hydrogen evolution experiment with GSH stabilized CdS Nanorods. Vertical line denotes energy of the excitation beam.

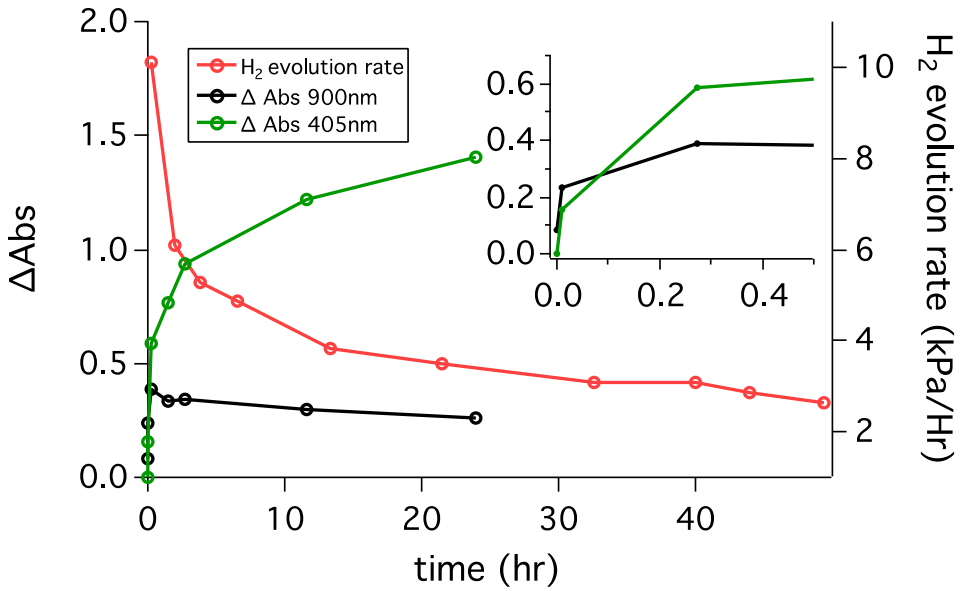

Figure SI.12B Correlation between decreasing H_2 evolution rate and increasing optical density at the excitation wavelength.

References:

1. J. H. Olshansky, T. X. Ding, Y. V. Lee, S. R. Leone and A. P. Alivisatos, *J. Am. Chem. Soc.*, 2015, **137**, 15567-15575.
2. R. R. Gagne, C. A. Koval and G. C. Lisensky, *Inorg. Chem.*, 1980, **19**, 2854-2855.
3. G. Rainò, T. Stöferle, I. Moreels, R. Gomes, J. S. Kamal, Z. Hens and R. F. Mahrt, *ACS Nano*, 2011, **5**, 4031-4036.
4. D. Steiner, D. Dorfs, U. Banin, F. Della Sala, L. Manna and O. Millo, *Nano Lett.*, 2008, **8**, 2954-2958.
5. A. Sitt, F. D. Sala, G. Menagen and U. Banin, *Nano Lett.*, 2009, **9**, 3470-3476.
6. A. Mirzahosseini and B. Noszál, *Sci. Rep.*, 2016, **6**, 37596.
7. F. Aldeek, M. Safi, N. Zhan, G. Palui and H. Mattoussi, *ACS Nano*, 2013, **7**, 10197-10210.
8. K. E. Sapsford, T. Pons, I. L. Medintz, S. Higashiya, F. M. Brunel, P. E. Dawson and H. Mattoussi, *J. Phys. Chem. C*, 2007, **111**, 11528-11538.
9. C.-H. Wu, P. M. McTernan, M. E. Walter and M. W. W. Adams, *Archaea*, 2015, **2015**, 8.
10. Z. Han, F. Qiu, R. Eisenberg, P. L. Holland and T. D. Krauss, *Science*, 2012, **338**, 1321-1324.